Process Safety and Environmental Protection 201 (2025) 107571

Contents lists available at ScienceDirect

Process Safety and Environmental Protection

journal homepage: www.journals.elsevier.com/process-safety-and-environmental-protection

Digital image processing for the advanced characterization and simulation of experimental fire tests

Alice Schiaroli [a,b], Christian Mata [c], Giordano Emrys Scarponi [a], Abdel Karim Habib [d], Martin Kluge [d], Federico Ustolin [b], Valerio Cozzani [a,*]

[a] LISES – Laboratory of Industrial Safety and Environmental Sustainability – Department of Civil, Chemical, Materials and Environmental Engineering, University of Bologna, via Terracini 28, Bologna 40131, Italy
[b] Norwegian University of Science and Technology (NTNU) - Department of Mechanical and Industrial Engineering, NTNU, Trondheim 7491, Norway
[c] Research Centre for Biochemical Engineering (CREB), Universitat Politècnica de Catalunya, Barcelona 08028, Spain
[d] Bundesanstalt für Materialforschung und –Prüfung, Unter den Eichen 87, Berlin 12205, Germany

ARTICLE INFO

Keywords:
Fire test
Digital image processing
Flame coverage
Fire engulfment
Boundary conditions
Storage tank

ABSTRACT

The fire engulfment of storage tanks of hazardous materials is among the most critical scenarios in hazard assessment of industrial value chains. Laboratory and full-scale experimental trials are used to test the tank performance and integrity in such scenarios. However, strong uncertainties usually affect the actual fire load experienced by the tank, in particular when large-scale experiments are carried out in open test fields. Such uncertainties arise from several factors difficult to control during experimental tests, such as the atmospheric conditions as there is the influence of wind drifts influencing the actual fire engulfment, the flame temperature and the flame dynamic distribution around the target. Consequently, verifying the concordance of an experimental test with standard test criteria and defining accurate boundary conditions in correlated model simulations is challenging. In this study, the development of a novel method for the analysis of fire conditions based on image processing is presented. The approach allows identifying the flame coverage on the target surface during the test and provides an accurate map of the flame distribution on the equipment over time. The approach is tested using experimental data from a full-scale fire test campaign carried out on liquid hydrogen cryogenic tanks. The results prove to be accurate in replicating the experimental temperatures measured on the outer tank shell during the test. The proposed methodology can be used to better understand the results of experimental fire tests and to characterize realistic fire scenarios, also supporting the definition of fire test requirements. Moreover, the approach produces results that can be implemented as advanced space-time-varying boundary conditions in simulation models, improving their accuracy in reproducing real cases.

1. Introduction

Lessons learned from past accidents evidence that fire engulfment and fire impingement pose safety-critical threats to storage and transport vessels of hazardous materials, in particular when considering pressurized or cryogenic liquefied gases (Hadjisophocleous et al., 1990a; Moodie et al., 1985; Scarponi et al., 2021; Wang et al., 2023). In such scenarios, the significant heat load provided by the fire can lead to catastrophic vessel failure due to mechanical stresses, resulting in dangerous events as fires, explosions, and a Boiling Liquid Expanding Vapour Cloud Explosion (BLEVE), with potentially severe consequences on people, environment, and assets (Birk, 1995; Birk and Cunningham, 1994). Thus, understanding the tank behaviour during fire attack is crucial to ensure the tank integrity, adopting robust design criteria and effective preventive and mitigative measures. This requires specific bench and full-scale experimental campaigns, usually feeding detailed modelling approaches. Regulations and codes were developed for vessel testing (American Petroleum Institute, 2014; Mutual, 1981; National Fire and Protection Association, 2011), and attempts were made to define minimum requirements for standardized fire test procedures ensuring the adequacy and significance of fire tests. Despite several criteria were developed to address the heat flux received by the tank and the level of fire engulfment, no internationally accepted fire test standardized methods still exist (Bradley et al., 2021).

* Corresponding author.
E-mail address: valerio.cozzani@unibo.it (V. Cozzani).

https://doi.org/10.1016/j.psep.2025.107571
Received 23 May 2025; Received in revised form 29 June 2025; Accepted 9 July 2025
Available online 10 July 2025

Actually, relevant differences are reported in the heat flow and engulfment level experienced by the vessels in different fire tests and experimental campaigns, as highlighted in Table 1, where some relevant experimental data retrieved from past fire tests are reported to exemplify the issue. All the fire scenarios considered in the table are pool fires.

The variability in the heat flux and engulfment conditions evidenced in Table 1 results from the variability of several external factors that influence these parameters, as, e.g., the atmospheric humidity, wind velocity, and drift. These factors, especially in outdoor tests, are difficult to control and change in different tests carried out in the same experimental set-up or even during a single test. Moreover, meteorological data are rarely measured and, even when available, their collection is not carried out by experts. As a consequence, uncertainties affect the actual test conditions and the fulfillment of the required nominal test criteria. On the one hand, this causes experimental data collection to be extremely challenging, due to the limited reproducibility of the experimental conditions. On the other hand, even when applying standardized test procedures, the validation of the results of experimental tests may be difficult due to the limitations in the assessment of the actual conditions occurring during the test.

Besides the formulation of standards, data from experimental tests were used in the past as the basis to validate mathematical models developed to investigate the fire engulfment of storage equipment, quantifying the tank pressurization, and estimating their thermal resistance. Once validated, the models were used to simulate various scenarios and analyse the influence of different parameters on the tank performance without the need for experimental tests, allowing to avoid the correlated costs, safety and environmental issues. In this context, the definition of accurate and realistic boundary conditions resembling the actual fire exposure is crucial to obtain reliable results. Unfortunately, since these conditions are meant to replicate the fire scenario, the uncertaintites discussed above affect their definition in modelling approaches, compromising the accuracy of the models.

Currently, in most of the available mathematical models, both analytical (Aydemir et al., 1988; Beynon et al., 1988; Birk, 1988; Bubbico and Mazzarotta, 2018; Graves, 1973; Hadjisophocleous et al., 1990b; Lautkaski, 2009; Leslie and Birk, 1991; Makarov et al., 2021; Moodie, 1988; Shebeko et al., 1996) and computational fluid dynamic (CFD) (D'Aulisa et al., 2014; Iannaccone et al., 2021; Scarponi et al., 2021, 2018a; Ustolin et al., 2022), a static full engulfment is considered. This conservative assumption reduces the complexity of the problem but does not consider the actual dynamic features of the fire, that several authors evidenced as crucial in determining the actual heat flux transferred to the vessel during fire tests (Bi et al., 2011; Hadjisophocleous et al., 1990a; Landucci et al., 2009; Scarponi et al., 2024; Sumathipala et al., 1992). Some studies addressed this issue by introducing partial engulfment scenarios (Bi et al., 2011; Birk, 2006; Hadjisophocleous et al., 1990a; Scarponi et al., 2018b, 2021; Yoon and Birk, 2004). However, in all these studies an empirical approach was used to determine the engulfed fraction of the vessel. Moreover, the latter was set constant throughout the simulations and only symmetric fire scenarios were considered. Therefore, to date specific methods for defining variable time and space-dependent boundary conditions for the standardized and reproducible modelling of full-scale fire tests are still missing.

A novel methodology for characterizing the fire engulfment of storage tanks involved in full-scale fire tests is proposed in this study. Unlike the abovementioned approaches, the new method allows for capturing the dynamic behaviour of the fire during experimental tests and replicating the non-uniform flame distribution around the vessel over time. This introduces a significant improvement with respect to the existing available methods, improving the accuracy of simulations and providing more accurate results.

The proposed method is based on Digital Image Processing (DIP), which is already widely applied for safety studies in several fields. A relevant example is the transportation sector, where DIP is used to monitor road conditions and identify dangerous imperfections (e.g., holes) (Eskandari Torbaghan et al., 2022), predict possible incidents based on traffic information (Huang et al., 2020) and analyse the driver's conditions that can potentially cause an accident (Alshaqaqi et al., 2013; Mu et al., 2022; Turan and Guota, 2013). A further example is the medical sector, where it is used since several decades for magnetic resonance or computerized tomography for disease detection and patient monitoring (Kansal et al., 2022; Mata et al., 2016). When considering fire safety, DIP has been used to better understand the flame features (e.g., by the analysis of flame colour and size) (Jie et al., 2018), providing information regarding the flame temperature and velocity (Rashidi et al., 2015) and the type of fuel (Zhou et al., 2014). Other applications include fire detection (Chi et al., 2015; Mahmoud and Ren, 2018; Manjunatha et al., 2015; Sharma et al., 2020) and characterization in terms of dimensions, location, emitted radiation, and flame velocity (Li et al., 2018; Mata et al., 2018). To date, DIP was not applied to the analysis of fire tests involving storage tanks.

In order to obtain more detailed data on actual engulfment and heat transfer in full-scale experimental fire tests, a novel DIP-based method for the analysis of the fire conditions is introduced. The method was applied to 2D frames extracted from conventional video recordings of experimental fire tests involving storage tanks. The procedure allowed the identification of the location of the flames on the target surface and to obtain 3D projection of the flame distribution, enabling to reproduce the fire engulfment occurring during the experimental test with a high precision. The accuracy of the approach was verified by carrying out a numerical thermal analysis on the 3D geometry of the tank to simulate its response during the fire attack. In the model, the boundary conditions representative of the fire engulfment were defined based on the flame distribution obtained from the DIP procedure. The results were then used to highlight the limitations introduced considering full static fire

Table 1
Examples of experimental data concerning the heat flux provided from the fire and engulfment conditions experienced in large-scale fire tests reported in the literature.

Vessel volume *(L)*	Wind effect	Fire black body temperature *(°C)*	Flame engulfment conditions	Heat flux from the fire *($W\,m^{-2}\,K^{-1}$)*	Reference
1890	Slight	800–900	25 % of total outer surface	According to fire black body temperature	(Birk et al., 2006)
1800	Slight	~ 880	Full	~ 110	(Prabhakaran et al., 2018)
3000	Significant	125–983	Partial	-	(Landucci et al., 2009)
	Slight	447–986	Uniform fire impingement	110	
4850	Significant	-	Partial (bottom part not covered by the flames)	63.3	(Droste et al., 2011)
4850	Slight	-	Full	90.2	
10,250	Slight	600 – 1050	Partial	85	(Moodie et al., 1988)
2500 – 20,000	-	800 – 900	-	81–135	(Droste et al., 2011)
128,000	Slight	650 – 990	-	51.5 – 99.6	(Townsend et al., 1974)

engulfment conditions, as commonly done when modelling experimental tests, evidencing the substantial improvement in the accuracy of the simulation obtained by the novel developed approach. The proposed methodology can also be used to quantify the engulfment fraction of the target and assess whether the minimum experimental test requirements are satisfied when considering the fire conditions. In addition, it can provide information to define additional criteria for the assessment of the test credibility based on an accurate characterization of the fire.

2. Methodology

A novel procedure was developed to obtain a digital map of the flames during a fire test. The procedure, referred to as FMIP (Flame Mapping through Image Processing) was developed to characterize the condition of a fire test and obtain a dynamic map of the flame distribution on the target object.

As mentioned, the FMIP method was based on digital image processing, consisting of image manipulation using a computer (Seeram, 2019). The DIP procedure is articulated in different consecutive steps, starting from the acquisition of the image into a computer and its conversion into a numerical matrix, *I(m,n)*, where each pixel is univocally identified and can be referred to as its 2D *(m,n)* indexes. Then, specific techniques (e.g., brightness and contrast increase) can be applied to improve the visual quality of the image (Singh and Mittal, 2014) and eventually to recover the original information biased by the presence of noises and blurs (Amudha et al., 2012). Depending on the software used for the analysis, a specific colour model (i.e., the model that defines how colours are converted into digital numbers) of the image must be used. Additional manipulations, such as the wavelet transform and morphological processing, can be applied to further reduce the information redundancy in the image, minimizing the memory needed for storage and the time required for further processing (Pitas, 2000). These techniques may be also used also to highlight the boundaries of elements facilitating their subsequent identification (Russ, 2006). Different approaches may then be used to separate, or segment, the parts of the image that are essential for the analysis from the non-relevant ones (Abubakar, 2012). For example, following a pixel-based method, the pixels in the image can be discriminated between "object pixels", that are of interest for the analysis, and the "background" based on a criterion for a specific pixel feature. Finally, the features of the boundaries and regions in the image (e.g., corners, shape) can be identified and used to distinguish and label the objects (Pitas, 2000).

The FMIP allows identifying and isolating the surface of the target covered by the flames at different times during the fire test, by processing frames extracted from the video recordings of the experiments. In the present analysis, the target was a storage tank engulfed in a fire during a fire test. Fig. 1 illustrates the workflow adopted in the analysis and the steps of the FMIP proposed for the characterization of the fire conditions.

Input data selection: The methodology is applicable to 2D images extracted from conventional video recordings of fire tests. Since the method aims at providing a 3D map of the flame over the outer surface of a tank engulfed in a fire, videos showing the tank from different perspectives (or views) are required to ensure that its entire surface is monitored during the test. The number of videos (*V*) depends on both the camera field of view and the tank orientation and shape, as these factors define how much of the tank surface can be captured in each video recording by a single camera. As an example, the camera arrangement around horizontal and vertical tanks in the fire tests used to test the results of the proposed method can be found in the Supplementary Material, Figure S1. To facilitate the image processing and ensure the best quality of the FMIP results, all the cameras should be placed at the same distance from the target. Moreover, all the videos should record in a synchronized manner to ensure temporal alignment across all data sources. The same frame rate (fps) should be used to allow the automatic extraction of frames. The use of high frame rates is

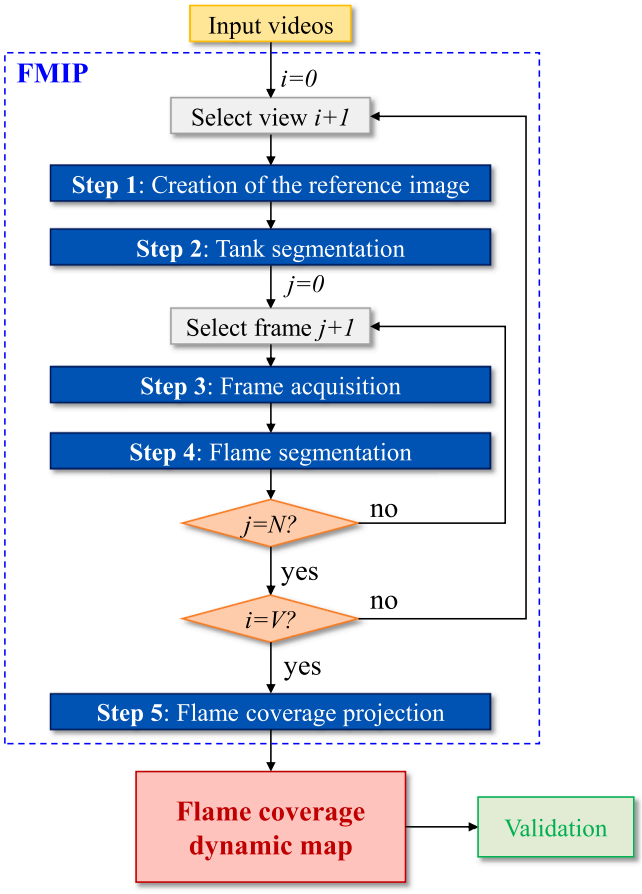

Fig. 1. Workflow of the methodology including the steps of the FMIP (Flame Mapping through Image Processing) developed.

recommended when a high level of detail is required in the analysis. Undesired objects (i.e., objects different from the target) between the camera and the target must be removed.

The number of frames (*N*) extracted for each recording is a choice of the analyst. The maximum value is limited by the frame rate of the camera and by computational resources required for the analysis, while the minimum is dictated by the time resolution required by the user. The frequency of frame extraction is selected depending on the specific application. It was demonstrated that extracting a frame each second gave highly accurate results for many studies (Leetaru, 2019).

Creation of the reference image: First, the tank should be isolated from the rest of the image in all videos. A frame capturing the tank before the beginning of the fire test is thus extracted from the video and converted into a 2D numerical matrix *I(m,n)*. Then, a Region of Interest (ROI) corresponding to the vessel section is defined, either manually or automatically (see the Supplementary Material, Table S1). Next, through a zeropadding process, the values of the pixels of the background (i.e., the pixels outside the ROI) are set to 0 and depicted as black, leaving the vessel section as the only visible object in the image.

Tank segmentation: The tank mask (i.e., a black and white image where the target is shown as white on a black background) is created assigning values to the pixels, based on their location in the image. This process, known as segmentation, is performed on the output of the previous step. First, the colour model is shifted from RGB (Red Green Blue) to CIE L*a*b standard (Plataniotis and Venetsanopoulos, 2000), where colors are expressed in terms of lightness (L) and two color dimensions representative of the color-opponent dimension of redness-greenness (a) and blueness-yellowness (b). Then, the k-means clustering pixel-based approach is used to obtain the tank mask (Jyoti

Bora and Kumar Gupta, 2014; Sinaga and Yang, 2020). The approach consists in an unsupervised algorithm which groups unlabeled data into clusters based on their similarity (Dhanachandra et al., 2015). Here, the similarity is established based on the pixel lightness so that all the pixels inside the ROI are included in the tank mask. The result is an image where the area inside the ROI (i.e., the tank section) is white (pixel value = 1) and the remaining part of the frame is black (pixel value = 0).

The next two steps of the FMIP are performed looping over the number of frames (*N*) extracted from the video recordings after the beginning of the fire test.

Frame acquisition: Different frames (*N*) showing the tank during the fire test are generated for the further analysis. The generic frame is extracted from the video, imported into the computer and converted into a 2D numerical matrix, as described for the creation of the reference image.

Flame segmentation: The flame mask is created with the same method illustrated for the tank mask. The tank mask obtained in Step 2 is overlapped to the frame extracted in Step 3 and all the pixels outside the tank mask are added to the background (i.e., depicted as black). Then, after the change of the colour model from RGB to CIE L*a*b, the flame is isolated from the tank using the k-means clustering approach. As in Step 2, the pixel lightness is used to discriminate between the pixels of interest and the rest (see Supplementary Material, Table S2).

In this step, the lightness criterion is chosen with the aim of dividing the fire from the tank surface not covered by the flame. The resulting image shows the flame as white on a black background. In numeric terms, the image corresponds to a 2D matrix, where the element ϕ_f is 1 if the corresponding pixel is covered by the flame, 0 otherwise.

Flame coverage projection: The 2D image of the flame coverage is projected on the 3D surface of the tank. Here, this was done using an orthogonal projection along the direction of the camera.

Once Steps 3–5 are completed for all the *N* frames of the selected video, the procedure is repeated for the next video, until the recordings (*V*) of all the views are processed. At the end of the procedure, a series of 3D flame coverage dynamic maps is obtained, covering the entire duration of the test. This is used in the validation phase, where the map is converted into the thermal boundary condition for the thermal analysis of the fire test.

3. Experimental test bed

Table 2 shows the experimental data used to define a test bed for the modelling approach developed. The data were obtained in three fire tests carried out at the Federal Institute for Materials Researching and Testing (BAM) in Berlin as part of the Safe Hydrogen Fuel Handling and Use for Efficient Implementation (SH2IFT) project (Ødegård et al., 2022).

In the experiments, three liquid hydrogen double-walled highly insulated cryogenic tanks with an inner volume of 1 m^3 (outer diameter = 1.35 m, length = 2 m) were exposed to an external propane fire. The inner (thickness = 3 mm) and the outer shell (thickness = 4 mm) of the three tanks were made of a stainless steel suitable for low-temperature applications (X5 CrNi 18–10). As shown in the table, different orientations (vertical or horizontal) and different thermal insulation materials (perlite or multi-layer insulation, MLI) were used. All the three tanks had an initial filling degree of about 35–40 %, corresponding to around 25–30 kg of liquid hydrogen. A total of 15 thermocouples were used for temperature measurements. Among them, 11 sensors were used to monitor the temperature of the outer tank shell: 6 were located in the middle of the tank surface (see green points in Fig. 3b), while the remaining 5 were positioned on top of the tank.

The propane used for the fire was supplied through 36 individual nozzles (12 ×3 grid) positioned under the tank and fed from a 5 m^3 propane tank via a liquid propane pump. Given the location of the nozzles, the fire resulted in a flame impingement scenario. The homogeneous heat load provided by the fire was estimated to be within the range of 100–150 kW m^{-2} at an average propane mass rate of 4.3 kg min^{-1} (Ødegård et al., 2022). The test BLEVE01 was manually stopped after a massive pressure loss was observed due to a leakage via the blind flange connection at a filling valve on top of the tank. The third test (BLEVE03) was also stopped manually when the propane tank feeding the burners was empty, while test BLEVE02 ended when the BLEVE occurred.

The input to the FMIP method developed are the videos recorded during the fire tests by four GoPro cameras located around the tanks. The frame rate of the recordings was 59.94 fps for BLEVE01 and BLEVE02 and 239.76 fps for BLEVE03. All the recordings had a Full High Definition (FHD, or 1080p) resolution; thus the extracted frames had 1920 horizontal pixels and 1080 vertical pixels (1920 ×1080, 16:9 aspect ration), resulting in a total of 2.07 million pixels per frame.

For each fire test, the video recordings were available from four views, namely East, West, North, and South; an example is shown in Fig. 2. However, in the case of the third test, the video recordings were available only for about half of the test duration (i.e., around 2 hours). Further details regarding the location of the cameras around the tank are reported in the Supplementary Material (see Figure S1). The frames were extracted with a frequency of 1 frame per second.

4. Modelling approach

To assess the accuracy of the proposed approach, the flame coverage dynamic map obtained from the FMIP of one of the tests was used to simulate the thermal response of the tank. BLEVE01 test was used to this purpose. The temperatures of the tank outer shell monitored at different locations during the test were compared with the results of the thermal analysis.

The software ANSYS Fluent 18.2 was used for the numerical thermal analysis (ANSYS Inc, 2018). The computational domain for the simulation was defined considering the geometry of the cryogenic double-walled insulated tank used in the test. The sole solid geometry of the tank (i.e., outer shell, insulation, and inner shell) was considered. No other components in the system (e.g., pipework, safety devices, etc.) were considered. The computational grid, shown in Fig. 3a, was obtained defining a maximum element size of 0.03 m for the tetraedric cells. Two finer meshes were also created to analize the grid independence of the results. The features of the two meshes are summarized in Table 3. The sensitivity analysis demonstrated the grid independence of the results of the thermal simulation (see Supplementary Material, Section 4.1). The results reported in the following are obtained with the M0 mesh (see Table 3).

Temperature-time curves were extrapolated from model results in correspondance of the fourteen monitoring points (MP) on the outer

Table 2
Description of the three fire tests carried out during the SH2IFT project (Ødegård et al., 2022); MLI = Multi-layer insulation; BLEVE = Boiling Liquid Expanding Vapor Explosion.

Test ID	Test duration *(min)*	Tank orientation	Tank insulation	Tank volume *(m^3)*	Filling degree *(%)*	Final event
BLEVE01	91	Horizontal	Perlite	1	35–40	Jet fire
BLEVE02	68	Horizontal	MLI	1	35–40	BLEVE
BLEVE03	240	vertical	Perlite	1	35–40	None

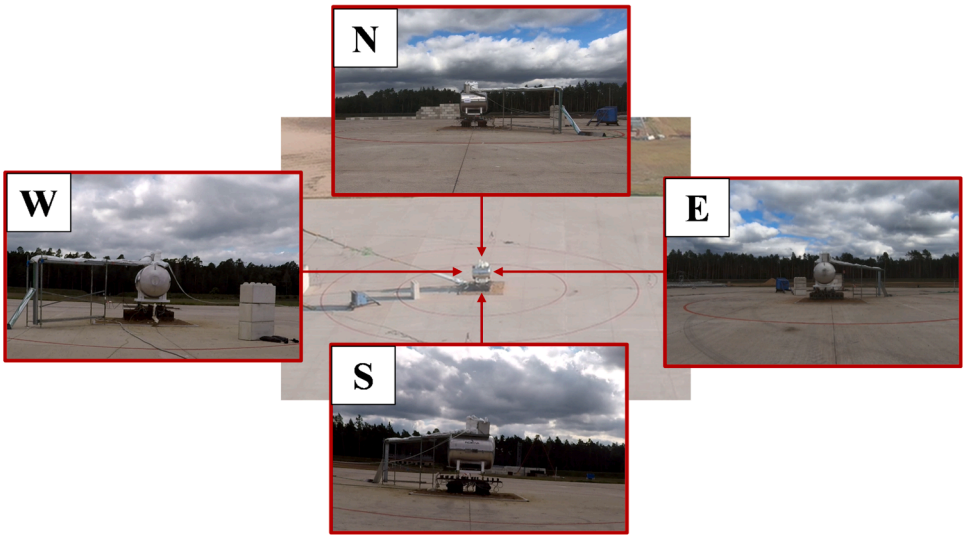

Fig. 2. Aerial and side views of the experimental setup used in the BLEVE02 test at the Federal Institute for Materials Researching and Testing, Berlin;(Abbreviations: E = East; N = North; W = West; S = South).

tank shell shown in Fig. 3b. A total of 6 monitoring points corresponded to the actual position of experimental sensors (i.e., green monitor points in Fig. 3b), thus allowing a direct comparison of model simulations with experimental data obtained by thermocouples. The other 8 monitoring points (black points in Fig. 3b) were virtual MP, only used to obtain relevant information concerning the model-predicted temperature-time trends in significant geometrical positions. The monitoring points were labelled based on their location of the tank surface. For a generic green label MP_X, X indicates the view (i.e., North, South, East, West, Down, and Up) in which the monitoring point was located. For the black points MP_X_Y, X had the same meaning as above, while Y specified the portion of the tank surface in the X specific view where the monitoring point was located. For instance, MP_N_east referred to the monitoring point located in the North view, in the eastern half of that surface. Heat flows at each side of the tank shells (i.e., inner and outer surface of each shell) were calculated in model simulations, based on the FMIP data.

The energy equation (Eq. 1) was solved within the domain during the simulation.

$$\frac{\partial(\rho C_p T)}{\partial t} = \nabla\cdot(k\nabla T) \tag{1}$$

Where ρ is the density in kg m^{-3}, C_p is the heat capacity in J kg^{-1}K^{-1}, T is the temperature in K and k is the thermal conductivity in W m^{-1}K^{-1}. For the insulation domain, the thermal conductivity of perlite of 0.016 W m^{-1} K^{-1} was defined based on the procedure described by Clark (1969) and considering an initial vacuum pressure of 0.3 mbar (Ødegård et al., 2022). The value was kept constant throughout the entire simulation, neglecting the possible degradation of the insulation system. The boundary conditions at the outer and the inner walls were defined according to Eq. 2 and Eq. 3, respectively.

$$q_{out} = \sigma\varepsilon_{w,out}\left(\varepsilon_{out}{T_{out}}^4 - {T_{w,out}}^4\right) + h_{out}(T_{out} - T_{w,out}) \tag{2}$$

$$q_{in} = h_{in}(T_{w,in} - T_f) \tag{3}$$

Where σ is the Stefan-Boltzmann constant (5.67×10^{-8} W m^{-2} K^{-4}), ε is the emissivity, T is the temperature in K, and h is the convective heat transfer coefficient in W m^{-2} K^{-1}. The subscripts w and f refer to the wall and fluid respectively, while the subscripts *out* and *in* indicate the outer and inner tank walls, respectively. The solver calculated the heat flux at the outer wall (Eq. 2) as a combination of convection and radiation. The outer temperature (T_{out}) at each point was defined by converting the flame coverage dynamic map (i.e., the output of the FMIP) into temperature profiles using Eq. 4.

$$T_{out} = \begin{cases} T_{flame}, & \phi_f = 1 \\ T_{amb}, & \phi_f = 0 \end{cases} \tag{4}$$

Where T_{flame} was the temperature of the flame and T_{amb} was the ambient temperature in K. In this way, a space-varying temperature profile was obtained for T_{out}, which was updated dynamically throughout the simulation with the same frequency used for the FMIP (once every second).

Based on the experimental data, the filling degree of the tank was set arbitrarily to the maximum possible value of 40 %. In the absence of direct flame temperature measurements, the radiative temperature (T_{flame}) was assumed and set to 1,193.15 K (Pehr, 1996), while a constant, average value of 293.15 K was considered for the ambient temperature due to its limited variation during the tests (±1°C). The emissivity of the surrounding (ε_{out}) and the outer wall ($\varepsilon_{w,out}$) were assumed to be 1, while the convective heat transfer coefficient (h_{out}) was set to 10 W m^{-2} K^{-1}. The heat transfer at the inner wall was assumed to occur by convection, as dictated by Eq. 3. The convective heat transfer coefficient (h_{in}) was defined with a user-defined function to distinguish between the liquid and vapour phases. Values of 10 W m^{-2} K^{-1} and 1 kW m^{-2} K^{-1} were selected for the inner tank wall above (i.e., gaseous hydrogen, red part of the inner wall in Fig. 3a, left) and below (i.e., liquid hydrogen, blue part of the inner wall in Fig. 3a, left) the liquid-vapour interface, respectively.

The initial condition was obtained as the result of a steady-state simulation reproducing the tank in normal operating conditions (i.e., before the beginning of the fire). The corresponding temperature distribution was calculated fixing $T_{out} = T_{amb}$ all over tha tank surface. A second order upwind discretization scheme was used to solve the energy equation; for the transient formulation, a first order implicit scheme was selected. A relative convergence criterion of 10^{-8} for energy was set for both the steady-state and the transient simulation.

To better understand the importance of the results obtained, a benchmark simulation was also carried out, by the introduction of a specific boundary condition considering a static full fire engulfment, as in state-of-the-art bench and full-scale fire test simulations. In the benchmark simulation, T_{out} was set equal to the T_{flame} all over the outer shell, and the latter value was considered constant throughout the entire simulation.

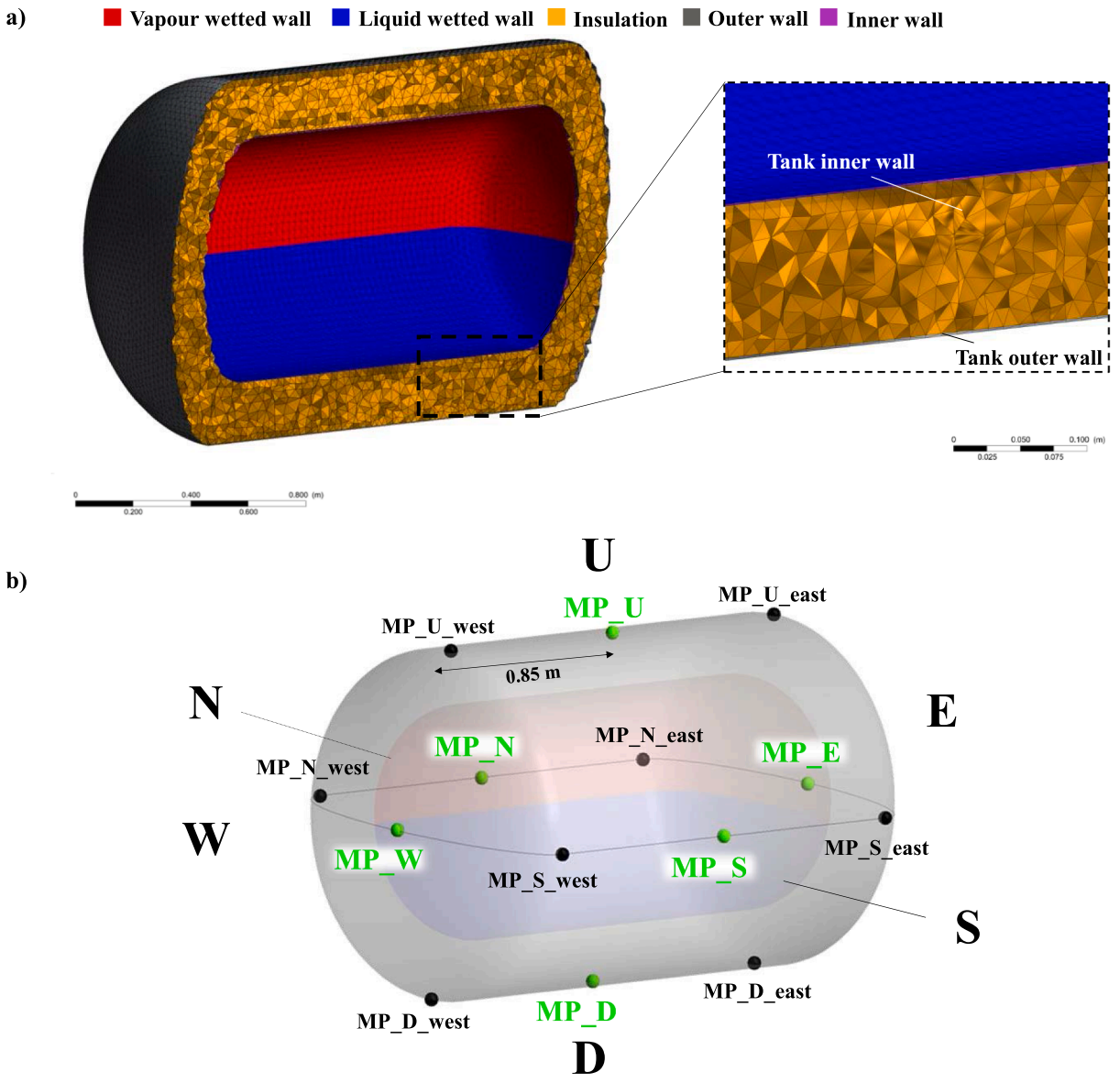

Fig. 3. a) Mesh of the computational domain used for the numerical thermal analysis; b) Location of the monitoring points on the outer shell of the tank: the green points represent the position of the experimental sensors used for temperature monitoring, located on the outer shell at the center of each view; the black points represent virtual monitoring points where simulated temperature-time curves were obtained from the model. D = Down; E = East; N = North; S = South, U = Up; W = West.

Table 3
Details of the computational meshes used to test the grid independency of the results.

Mesh	Mesh ID	Element type	Number of elements	Element size (m)
Original mesh	M0	tetrahedrons	496,501	0.030
1st refined mesh	M1	tetrahedrons	1129,559	0.025
2nd refined mesh	M2	tetrahedrons	2141,659	0.020

5. Results and discussion

5.1. FMIP (Flame Mapping through Image Processing) results

An example of the results of the FMIP is shown in Fig. 4. Fig. 4a and Fig. 4b show the steps for the creation of the tank (Step 2 in Fig. 1) and flame (Step 4 in Fig. 1) masks for the South view of the tank used in BLEVE02 test. In the final mask, the object of interest (the tank in Fig. 4a and the flame in Fig. 4b) appears in white on a black background.

The flame mask shown in Fig. 4b represents the fire engulfment of the tank after 170 seconds from the beginning of the fire test. Even if the single frame is not representative of the overall average fire engulfment, it clearly shows that the level of engulfment was lower than 100 %. Moreover, in the selected frame, the flame appeared to be shifted to the left, a distinctive evidence of the presence of considerable wind blowing towards West. Similar results were obtained for the other views, confirming that the full engulfment simplification does not realistically reproduce the test conditions and proving that the wind significantly influences the flame distribution around the tank.

Once the flame masks for all the frames were obtained, the flame coverage of the tank (i.e., fraction of the outer tank surface covered by the flame during the fire test) at a fixed time ($\Phi_f(t)$) and the average flame coverage during the test (φ_f) were calculated using Eq 5 and Eq. 6:

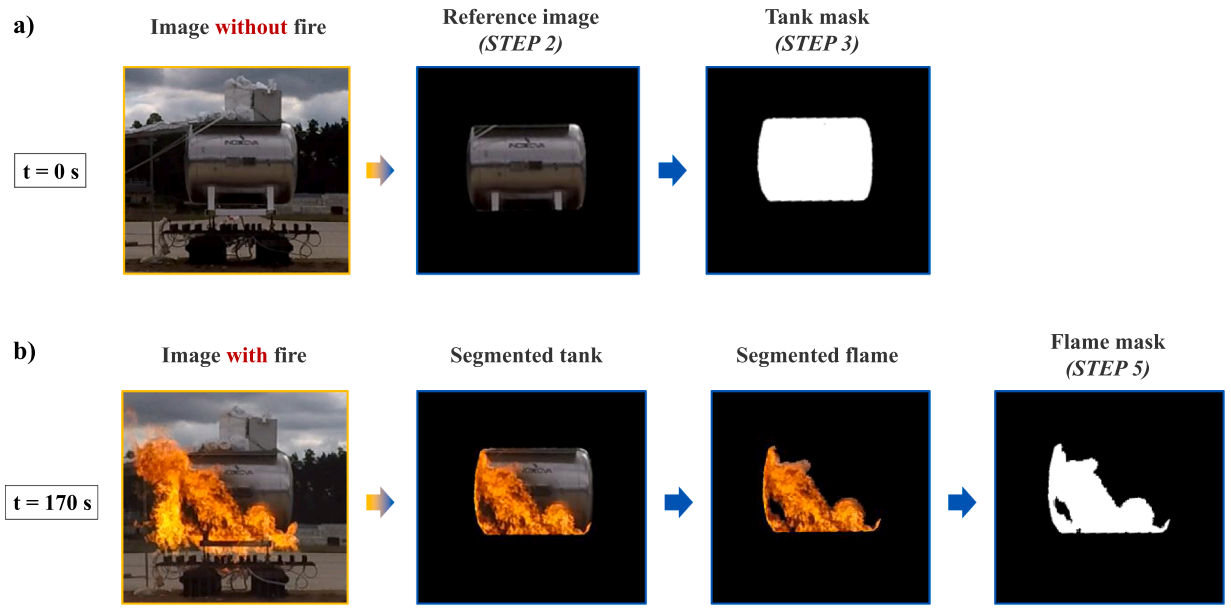

Fig. 4. Results obtained from the application of the FMIP approach on the frames of the South view of BLEVE02 fire test; a) steps for the creation of the tank mask; b) steps for the creation of the flame mask 170 seconds after the start of the fire test. The steps of the procedure are summarized in Fig. 1.

$$\Phi_f(t) = \int_{A_{tank}} \phi_f(t)dA \quad (5) \qquad \varphi_f = \int_{t_{test}} \Phi_f(t)dt \quad (6)$$

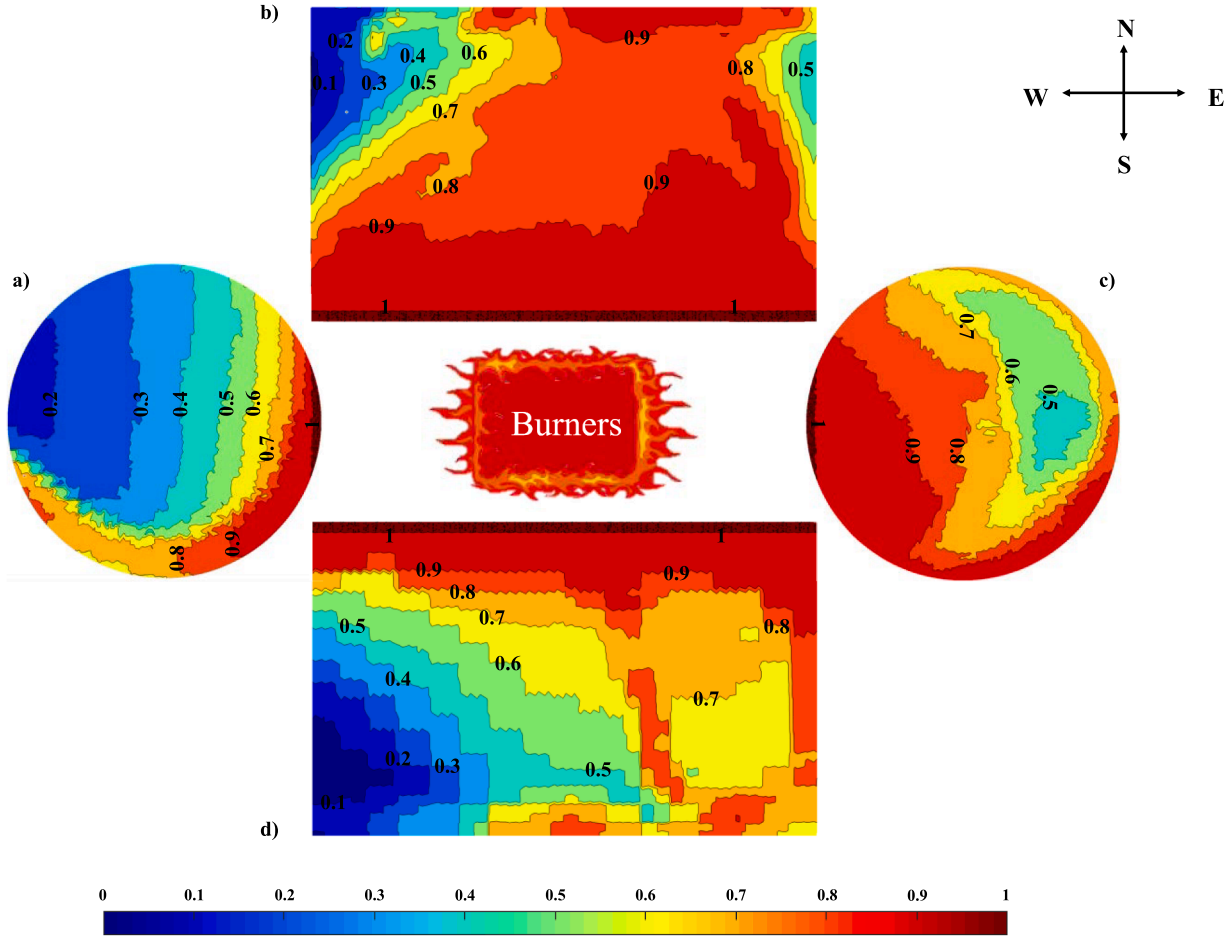

Fig. 5. Flame coverage on the four views of the tank calculated for the entire duration of BLEVE01 test; a) West view; b) North view; c) East view; d) South view.

Where A_{tank} is the outer surface of the tank and t_{test} is the duration of the fire test.

Significant differences were obtained in terms of average flame coverage for the three tests: 68 % for BLEVE01, 37 % for BLEVE02, and 11 % for BLEVE03. The relevant discrepancies between the results of the horizontal tanks (BLEVE01 and BLEVE02) indicate that, despite the same experimental set-up, the weather conditions during the two tests changed considerably leading to different engulfments. The lowest

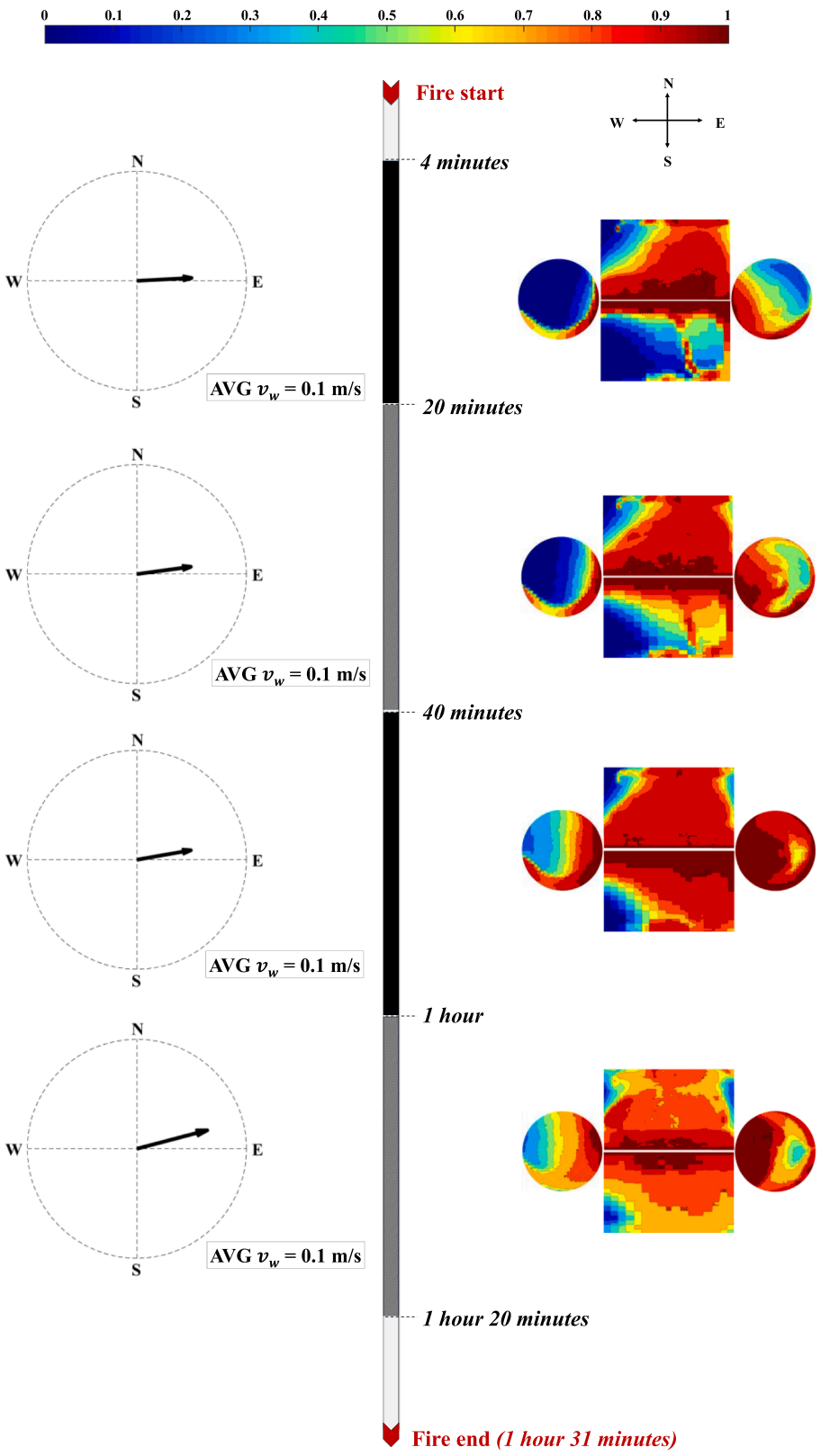

Fig. 6. Correlation between wind direction, average wind velocity (AVG v_w) and flame coverage calculated every 20 minutes during fire test BLEVE01; experimental data are available starting from 4 minutes from the test start. The tank surfaces are oriented as indicated by the cross at the top, coherently with Fig. 5.

average flame coverage obtained for BLEVE03 can be explained by considering the different tank orientation: in tests BLEVE01 and BLEVE02 the tank was positioned horizontally and part of the cylindrical shell was directly above the fire burners while in the vertical configuration a smaller surface (tank head) was directly exposed to the burners and the furtherst extent of the tank was much more distant from the burners.

The average flame coverage obtained for the four views of the tank in BLEVE01 test is illustrated in Fig. 5. As expected, the areas of the tank nearest to the burners were the zones where the flame was more consistently present. The results obtained demonstrate that the flame distribution around the tank was strongly heterogeneous in both the horizontal and vertical direction, with some areas almost not covered by the fire.

This inhomogeneous distribution of the flame can be attributed to the influence of the wind, as shown in Fig. 6, where the flame coverage of the four views calculated every 20 minutes is correlated with the measured wind velocity and direction. The wind data are correlated with the average flame coverage (φ_f in Eq. 6) for all the tests in Table 4. The table also reports the standard deviation of the flame coverage, reflecting the relevance of the time variation of flame coverage.

As anticipated above, relevant differences were found between BLEVE01 and BLEVE02 (see Table 4 and maps reported in Figures S2 and S3 of the Supplementary Material). These may results from different wind velocities, which can affect the flame height. As wind speed increased, the lift-off of hot gases by natural convection was hampered, causing the flame to become shorter and more stretched in the horizontal direction rather than rising vertically. Thus, the level of engulfment was reduced, as in the case of test BLEVE02 (see Supplementary Material, Figure S2). In the case of BLEVE03 the effect of the highest wind velocity combined with the tank orientation contributed to further reduce the flame coverage, as shown in Table 4 and in Figure S3 in the Supplementary Material. A higher variability of the average flame coverage over time in the test BLEVE03 was also evidenced by the higher value of the standard deviation, which reflects the higher wind variability recorded.

The results obtained clearly show the complexity behind the characterization of the fire during fire tests. Moreover, they clearly indicate that the assumption of a static full fire engulfment is highly unrealistic and inadequate to reproduce the flame coverage of the tanks during the tests, as it neglects the influence of wind on the level of engulfment of the targets.

5.2. Numerical thermal analysis of fire tests and benchmarking with full engulfment fire scenario

Fig. 7 shows the comparison of numerical thermal analysis with the temperature values on the outer tank wall measured by the thermocouples (green points in Fig. 7a) during BLEVE01 test. In the figure, the results obtained from the simulation (green curves) are compared with available experimental data (black curves) measured during the fire test and with the results of the benchmark simulation obtained considering full engulfment conditions (red curves).

The comparison of the temperature trends with the experimental data highlights the capability of the proposed approach to provide more realistic boundary conditions for modelling the effect of flames on tanks in a fire. Overall, even in the presence of errors, the trend of the experimental curves was well replicated using the novel FMIP approach developed, with temperature peaks and lows calculated at the correct time. In contrast, the static full engulfment condition provided a single temperature-time profile across the entire tank, neglecting the localized temperature changes and variable flame distribution. For the Down view (Fig. 7e) the curves of the two approaches overlapped because, being that surface upon the burners in direct contact with the fire, its temperature equals the flame temperature in both cases.

A more detailed analysis of the results reported in Fig. 7 evidenced that for some monitoring positions, the results were very close to experimental data (e.g., MP_S, related to the South view in Fig. 7d) while in other cases the values were higher than the experimental ones, even if the overall trend was the same. For instance, as clearly visible from Fig. 7b (MP_W, related to West view), the dynamic behaviour of the experimental curve was very well reproduced in the simulation, but the calculated temperature values were always higher than the experimental ones, with a difference of about 200 K. Similar observations can be done for the MP_N monitoring point (Fig. 7c). The differences detected in the temperature values can be attributed to neglecting the effect of flame transparency on the flame temperature. As mentioned above, a single value for the flame temperature was selected, considering the mean fire temperature measured in the BMW fire tests (Pehr, 1996). However, this was a strong simplification of the real scenario, where the flame exhibited different colours and optical thicknesses, and did not have a constant distance from the target, resulting in a range of temperatures rather than a single constant value. Additional factors, such as neglecting the cooling effect of both the external wind and internal fluid, the inertia of the measuring equipment, and the type of fixation used to place the thermocouples on the tank surface can play a role. The results obtained suggest that the flames covering the West (related to MP_W, Fig. 7b) and South surfaces (related to MP_S, Fig. 7d) had a different optical thickness. Specifically, they indicate that the West surface was covered by an optically thin flame, with a lower equivalent black body and convective temperature than what assumed in the analysis, while a thicker flame was present on the South surface. Moreover, the results obtained for MP_D (Fig. 7e), which was directly above the burners, suggest that the real equivalent black body and convective temperature of the flame was lower than the value considered in the simulations. Finally, it should be remarked that major discrepancies between the calculated and experimental values were found for MP_U (Fig. 7f). These can be attributed to the neglection of the distance between the flame and the target.

It is worth to remark that the results of the temperature trends shown in Fig. 7 are coherent with the flame coverage illustrated in Fig. 5. The flame temperature was quickly approached in the MP_S, MP_E, and MP_D monitoring points (positioned in the center of the South, East and Down views respectively, as shown in Fig. 7), where the flame coverage was the highest, while a slower heating of the outer tank wall was observed in monitoring points MP_W, MP_N, MP_U, where the flame coverage was lower. It is important to mention that, after the test, a significant deformation was observed in the North surface of the tank, possibly influencing the flame distribution around the component.

Fig. 8 shows the temperature measured in correspondence of the

Table 4
Duration, average flame coverage, standard deviation and wind data of the three reference fire tests (AVG = average; SD = standard deviation).

Test ID	Test duration *(min)*	Number of extracted frames	AVG wind direction*	AVG wind velocity *(m/s)**	AVG flame coverage (φ_f)	AVG SD of flame coverage
BLEVE01	91	5456	East	0.11	0.72	0.1669
BLEVE02	68	3737	West	0.89	0.46	0.0795
BLEVE03**	120	7272	West	1.00	0.41	0.0912

* data available every 10 min
** data recordings were available only for 120 min although test duration was 240 min.

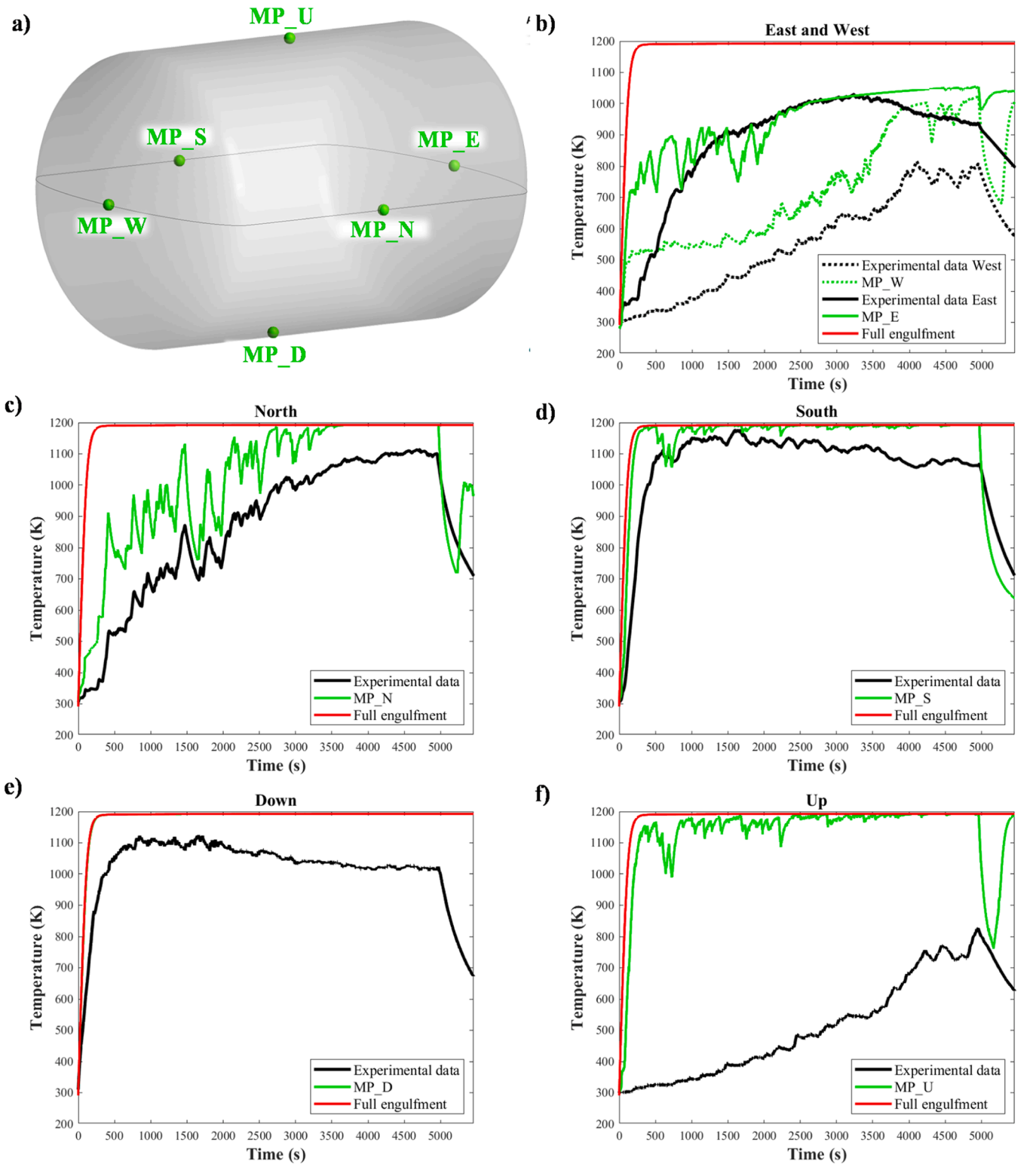

Fig. 7. Comparison of numerical thermal analysis obtained considering FMIP and full engufment boundary conditions with experimental temperature data available for the BLEVE01 test: a) Position and tag of the monitor points (see further details in Fig. 3b); b) MP_E and MP_W monitoring points; c) MP_N monitoring point; d) MP_S monitoring point; e) MP_D monitoring point; f) MP_U monitoring point.

virtual monitoring points (black points in Fig. 8a).

As shown in the figure, relevant differences were present between the temperatures of the monitoring points in the West and the East zones of the tank surface. The average temperature calculated at MP_N_west is 850 K, lower than the value of about 1000 K obtained at MP_N_east. Since the horizontal distance between the two monitoring points was 0.85 m (see Fig. 3b), the temperature increased with an average gradient of 176 K/m between the West and East zone. Similar observations apply for the other views. In the case of the tank heads, the temperature measurements were clearly influenced by the height of the monitoring point (Figure S6 in the Supplementary Material). The inhomogenity of the temperature of the outer tank shell well reflected that of the flame

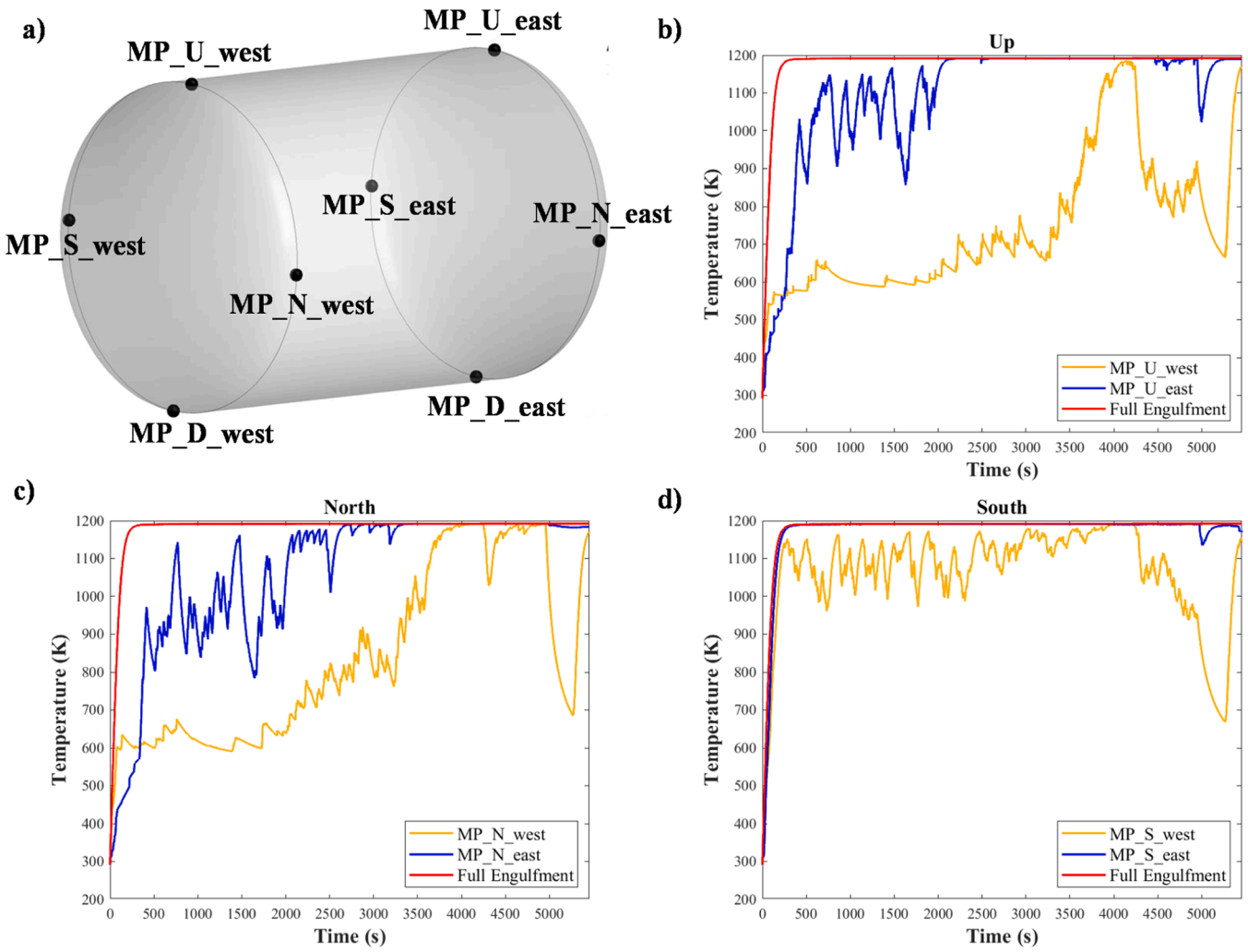

Fig. 8. Comparison of the results of numerical thermal analysis of the BLEVE01 test, obtained by FMIP and full engufment boundary conditions at the virtual monitoring points considered in Fig. 3: a) Position and tag of the virtual monitoring points; b) MP_U_west and MP_U_east; c) MP_N_west and MP_N_east; d) MP_S_west and MP_S_east.

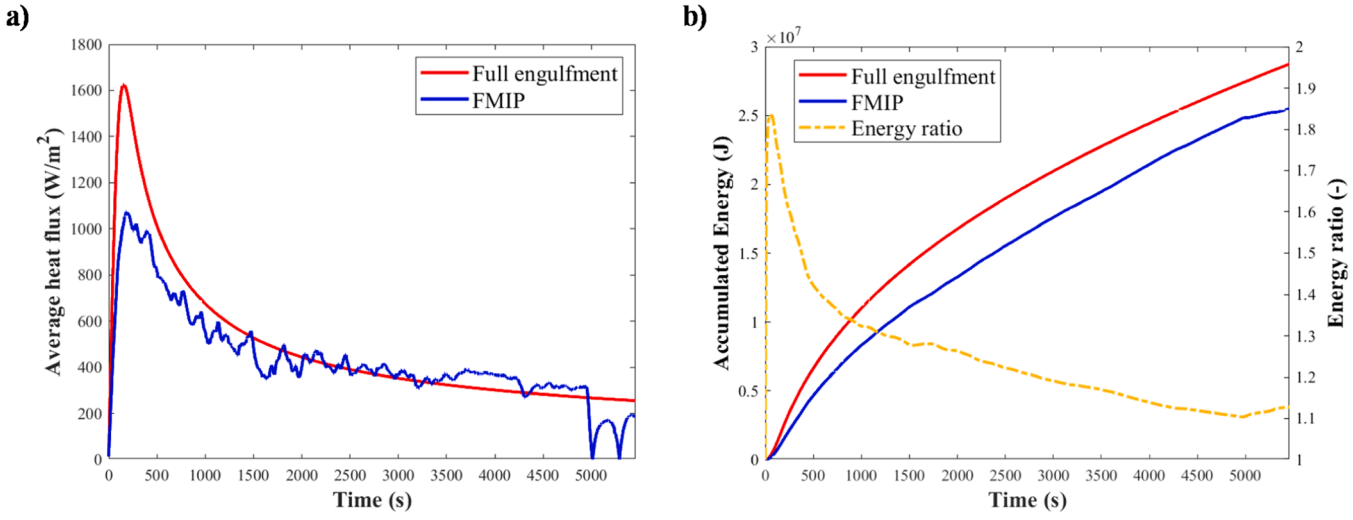

Fig. 9. a) Average heat flows at the inner surface of the tank outer shell applying the full engulfment and the FMIP conditions; b) Energy accumulated at the inner surface of the tank outer shell, calculated using the full engulfment and the FMIP conditions. The energy ratio, calculated dividing the energy estimated by the full engulfment assumption by the energy obtained by the FMIP methodology is also reported. All the curves were calculated considering a thermal conductivity value of 0.016 W m^{-1} K^{-1} for the perlite insulation present between the inner and outer vessel.

distribution around the vessel (see Fig. 5). As discussed before, during the experimental test the flame mainly covered the East area of the tank, quite uniformly, while the coverage in the West area was lower and not homogeneous. These results highlight the high variability of the temperature trends along the tank length, emphasizing the importance of a properly designed experimental set-up to capture meaningful data on the actual heat-up and heat flux entering the vessel.

When considering the differences among the results of the FMIP and benchmark simulations, similar results are obtained in Fig. 7 and Fig. 8. More specifically, very similar results were obtained for the FMIP and benchmark simulation in the case of MP_D (Fig. 7e), which was representative of the area of the tank surface always in contact with the fire: the temperature-time curves were perfectly overlapped and the maximum temperature is reached almost immediately. A good agreement among the FMIP and benchmark simulations was obtained at MP_S (Fig. 7d), MP_S_east (Fig. 8d), MP_S_west (Fig. 8d), and MP_E (Fig. 7b). In contrast, relevant differences between the static full engulfment and dynamic partial flame coverage were found for the MP_N (Fig. 7c), MP_N_east (Fig. 8c), MP_N_west (Fig. 8c), MP_W (Fig. 7b) and MP_U (Fig. 7f) monitoring points. Overall, the benchmark full engulfment hypothesis results were overconservative, leading to considerably higher heat flows than those actually occurred in the tests.

Fig. 9 shows the calculated heat flows across the vessel shell and the energy accumulation at the inner surface of the tank outer shell (i.e., surface of the outer shell in contact with the insulation) obtained from the thermal analysis of the BLEVE01 test considering either the FMIP or the full engulfment boundary conditions.

Since the tank was highly insulated (k=0.016 in Eq. 1), negligible differences in the heat flux transferred to the fluid were obtained with the two approaches. In contrast, as shown in Fig. 9a, discrepancies between the average heat flux calculated at the inner surface of the tank outer shell were observed. A maximum difference of 635 W m^{-2} was obtained after 157 seconds, coinciding with the peak in the heat flow. After that, the curves tended to overlap. As a result, the energy accumulated, calculated as the integral of the heat flux over time, was always higher when the full engulfment assumption was considered, as shown in Fig. 9b. Moreover, the results of the energy ratio (i.e., the ration between the energy accumulated under the full engulfment assumption and the energy accumulated considering the dynamic flame coverage) indicate that, at the beginning of the test, the energy calculated with the full engulfment assumption was nearly double (1.83) the one calculated with the dynamic flame coverage. Then, the ratio gradually decreased, coherently with the discrepancies in the heat flux trends. However, a 10 % difference persisted.

It is worth noting that these results are referred to the test BLEVE01, for which the highest average flame coverage was obtained (Table 4). Even more significant differences in the heat flows and accumulated energy are expected when considering scenarios with lower flame coverage, i.e., BLEVE02 and BLEVE03.

6. Discussion

The results of the present study show that the FMIP methodology allows a more realistic characterization of the actual fire coverage conditions during fire tests, accounting for the dynamic nature of the fire. The comparison with the results obtained for the benchmark case considering full engulfment shows that the latter can be extremely conservative and far from real fire conditions, in particular when considering fire tests carried out in the open air. In these tests, the presence of the wind plays a significant role in the flame distribution around the target, causing time variable and inhomogeneous conditions in the presence of wind drifts and high wind velocities. Moreover, the results show that the assumption of full engulfment conditions leads to an overestimation of the heat flux received by the target, possibly leading to an incorrect prediction of the tank thermal response.

The accuracy of the thermal analysis based on the boundary conditions obtained by the FMIP model can be further improved, when addressing a few specific additional factors.

First, the image quality is of paramount importance. This includes the contrast of colours in the images, the positioning of the cameras around the target, and the presence of undesired objects. Regarding the first point, a high colour contrast should be ensured to facilitate image segmentation using pixel lightness as a discriminating criterion. In relation to the second aspect, special attention should be paid to the positioning of the cameras to avoid overlapping fields of view. This can lead to double-counting of the same surface area once the flame masks are projected from 2D (Step 4) to 3D (Step 5). This issue is evident when comparing the average flame coverage φ_f of the tanks calculated based on the 3D projections of the flame masks on the tank outer wall (BLEVE01_3D, BLEVE02_3D, BLEVE03_3D) and directly considering the 2D masks obtained in Step 4 (BLEVE01_2D, BLEVE02_2D, BLEVE03_2D), as shown in Fig. 10. Small differences waere obtained for the first two tests, where the tank was oriented horizontally. Specifically, an increase in the average flame coverage of 3 % and 9 % (passing from 2D masks to 3D projections) was found for BLEVE01 and BLEVE02, respectively. For BLEVE03 test, where the tank was vertical, the result of the 3D calculation was 66 % higher than the one obtained with the 2D frames.

The small differences in the results obtained with the two methods for tests BLEVE01 and BLEVE02 can be attributed to the variation of the object dimension between Step 4 (2D masks) and Step 5 (3D flame maps). In fact, given the cylindrical shape of the tank, the pixels projected in the proximity of the curvatures have a higher weight in the calculation while in the second method all the pixels in the mask correspond to the same surface area. Thus, small differences in φ_f calculated in 3D and 2D depend on the extent of the flame in the higher curvature regions. However, the bigger discrepancies in test BLEVE03, highlight the impact of the extensive overlap between the cameras fields of view which resulted in a significant redundancy in the captured flame regions (see Figure S1 in the Supplementary Material). These results suggest that, the placement of the cameras used in the reference tests was adequate for the horizontal tanks. In contrast, a different configuration should be implemented to record the tests involving the vertical vessel. This can be defined following suggestions available in the literature (Kim and Jo, 2023; Olague and Mohr, 2002; Rahimian and Kearney, 2017).

In addition to the relative camera placement, it is important to avoid variations of the position of the cameras during the recordings, to ensure the automatic definition of the region of interest and allow for effective

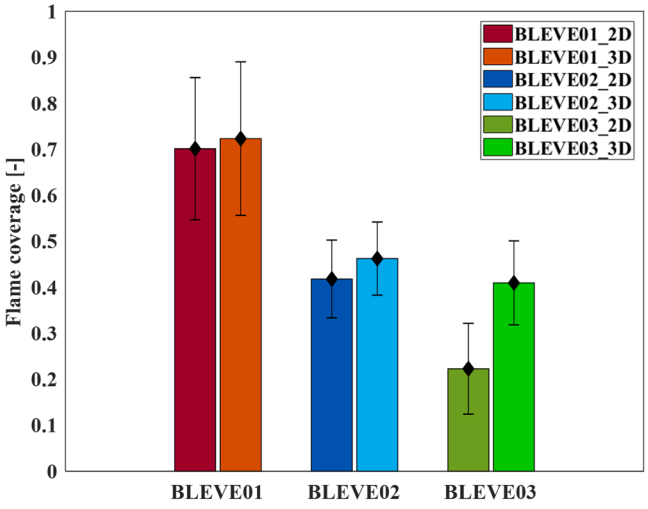

Fig. 10. Comparison of the average flame coverage (colored bars) and its standard deviation (black hyphens) calculated for the three fire tests BLEVE01, BLEVE02, and BLEVE03 considering the 2D flame masks (Step 4 of the FMIP) or the 3D projections (Step 5 of the FMIP).

image processing. If that is not the case, multiple regions of interest must be defined for a single view to create the reference image, even if this will result in a time-consuming process. In the experimental fire tests, the cameras did not move during the test. However, the field of view of one of the cameras accidentally shifted in test BLEVE02, requiring the definition of two region of interest (see the Supplementary material, Table S1). The cameras need to be placed at the same distance from the target in all the directions, so that the surfaces of the component shown in opposite views (e.g., East and West) have the same sizes and can be isolated with the same ROI.

Finally, the number of objects that are not of interest to the analysis (i.e., different from the target) between the target and the cameras should be minimized to avoid the alteration of the masks. An example of this issue is shown in Fig. 11, where a pipe of the experimental setup is included in the flame mask.

The characterization of the fire is another crucial aspect. The image processing was performed on 2D images showing a specific tank surface covered by the flames (e.g. see the first images in Fig. 4a and Fig. 4b). Thus, no information regarding the distance between the flames and the tank outer surface was extracted, leading to an overestimation of the tank outer temperature in some regions (e.g., Up view, see Fig. 7f). In perspective, videos recorded from above the tank could help to address this limitation. However, this is hardly feasible due to issues with the setup required to place the camera above the tank (e.g., uncertainty about how to hold the camera, possible damage due to fire radiation, possible partial shielding due to smoke, etc.). Alternatively, thermocouples placed at different distances from the tank may be added to the experimental setup, allowing the definition of a variable flame intensity, which could improve the accuracy of the temperature profiles. Directional flame thermometers may also be included in the setup to estimate the flame temperature (both equivalent black body and convective), as done in some past fire tests (Bradley et al., 2021).

Moreover, in addition to the application shown in the present study, in perspective the novel FMIP methodology introduced may be used to support the definition of standardized fire test procedures. Actually, the fundamental requirements currently available in the literature to assess the validity of a fire test have been defined based on the evidence of past experimental campaigns testing pressure vessels in fire conditions. These requirements include the range for the net heat flux transferred from the fire, the level of engulfment, the type of heat source (e.g., burners fed with liquid propane or butane), and the management of the wind against which a certain resistance should be ensured (Bradley et al., 2021). The application of the FMIP approach may simplify the estimation of all these data, that are typically difficult to collect. First, the heat flux received by the component and the average flame coverage can be estimated and compared with the thresholds once the external temperature profiles are defined. Then, the resistance of the flame to the wind can be verified observing the variability of the flame coverage with the wind orientation and velocity during the test, similarly to what is shown in Fig. 6.

Finally, the results achievable with the FMIP methodology can provide the basis for an improved assessment of the data from fire tests, also allowing a more confident comparison of different experimental runs. Since various factors often make it difficult to conduct tests respecting the desired nominal parameters (e.g., a specific level of engulfment of the target), interpreting the experimental data could be difficult due to the uncertainties on the actual test conditions. Furthermore, when comparing data from different tests, the causes of eventual differences may not be clear. For instance, if the pressurization of tanks differs between two tests, it might be uncertain whether this discrepancy is due to a different level of engulfment or to other factors (e.g., a difference in the performance of the insulation system for the case of cryogenic tanks). The quantification of the flame coverage of the targets with the FMIP may support the post-processing of the test outcomes, providing information for an objective in-depth analysis of experimental results and their comparison with other experimental data. Moreover, even when the actual test conditions differ from the nominal ones, the method allows data analysis, which normally would be hampered, avoiding the need of multiple test repetition.

Ultimately, correlations between the flame coverage of the equipment and relevant external factors can be defined combining the flame map with environmental data, as done with the wind direction and velocity in this study, allowing in perspective the introduction of new acceptance criteria for fire test in different environmental conditions.

7. Conclusions

A digital image processing methodology was developed to analyse fire tests involving storage tanks to provide more realistic boundary conditions for the modelling of tanks in a fire. The method allows defining the dynamic fire coverage of the involved component during the fire attack and replicating its thermal response. A strong correlation of the flame distribution around the tank with the wind features (direction and velocity) was demonstrated, emphasizing the importance of considering the ambient conditions when replicating the real scenario during modelling. The influence of wind drift and wind velocity on the actual flame coverage and heat flow to the vessel were clearly evidenced by benchmarking the results of the modelling approach developed to full engulfment conditions.

Overall, the results of the present analysis highlight crucial aspects that need to be considered in the design of the experimental set-up of future fire tests for storage tanks. A specific strategy is suggested for the displacement of videocameras in order to obtain qualified data for the application of the methodology, that may be integrated to the specific design of the matrix of thermocouples needed for appropriate temperature monitoring. The proposed approach can contribute to the development of standardized fire test procedures, allowing the verification of minimum requirements for the fire test quality. The methodology may thus support and facilitate the definition of internationally recognized fire test standards and procedures.

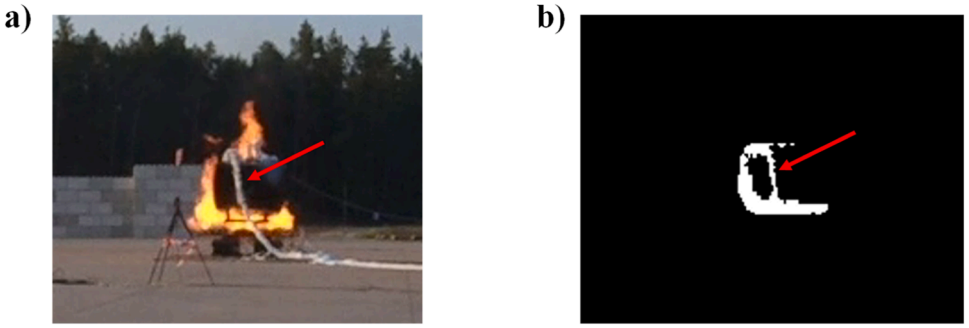

Fig. 11. Example of alteration of the flame mask due to undesired objects placed between the target and the camera for test BLEVE01, South view: (a) image of the fire; (b) corresponding flame mask.

CRediT authorship contribution statement

Alice Schiaroli: Writing – original draft, Methodology, Investigation, Formal analysis, Data curation, Conceptualization. **Christian Mata:** Software, Methodology, Investigation, Conceptualization. **Giordano Emrys Scarponi:** Writing – original draft, Supervision, Methodology, Investigation, Conceptualization. **Habibd Abdel Karim:** Investigation, Formal analysis, Data curation. **Martin Kluge:** Investigation, Formal analysis, Data curation. **Federico Ustolin:** Writing – review & editing, Supervision, Conceptualization. **Valerio Cozzani:** Writing – review & editing, Supervision, Methodology, Conceptualization.

Declaration of Competing Interest

The authors declare that they have no known competing financial interests or personal relationships that could have appeared to influence the work reported in this paper.

Acknowledgements

This work was undertaken as part of the research project Safe Hydrogen Fuel Handling and Use for Efficient Implementation 2 (SHIFT-2), and the authors would like to acknowledge the financial support of the Research Council of Norway under the ENERGIX programm (Grant No. 327009). This work was undertaken as part of Project "NEST - Network 4 Energy Sustainable Transition", PE000000214, CUPJ33C22002890007 funded by the Italian Ministry of University and Research under the National Recovery and Resilience Plan, Misson 4, Component 2, Investment 1.3, NextGenerationEU. This work was undertaken as part of the ELVHYS project No. 101101381 supported by the Clean Hydrogen Partnership and its members. UK participants in Horizon Europe Project ELVHYS are supported by UKRI grant numbers 10063519 (University of Ulster) and 10070592 (Health and Safety Executive). Funded by the European Union. Views and opinions expressed are however those of the author(s) only and do not necessarily reflect those of the European Union or Clean Hydrogen JU. Neither the European Union nor the granting authority can be held responsible for them.

Appendix A. Supporting information

Supplementary data associated with this article can be found in the online version at doi:10.1016/j.psep.2025.107571.

References

Abubakar, F.M., 2012. A study of region-based and contourbased image segmentation. Signal Image Process. Int. J. 3, 15–22. https://doi.org/10.5121/sipij.2012.3602.
Alshaqaqi, B., Baquhaizel, A.S., Ouis, M.E.A., Boumehed, M., Ouamri, A., Keche, Mokhtar, 2013. Driver drowsiness detection system. 8th Int. Work. Syst. Signal Process. Appl.
American Petroleum Institute, 2014. API Standard 521: Pressure-relieving and Depressuring Systems.
Amudha, J., Pradeepa, N., Sudhakar, R., 2012. A survey on digital image restoration. In: Procedia Engineering. Elsevier Ltd, pp. 2378–2382. https://doi.org/10.1016/j.proeng.2012.06.284.
ANSYS Inc, 2018. Ansys Fluent User Guide, Release 18.2.
Aydemir, N.U., Magapu, V.K., Sousa, A.C.M., Venart, J.E.S., 1988. Thermal response analysis of LPG tanks exposed to fire. J. Hazard. Mater. 20, 239–262.
Beynon, G.V., Cowley, L.T., Small, L.M., Williams, I., 1988. Fire engulement of LPG tanks: heatup, a predictive model. J. Hazard. Mater. 20, 227–238. https://doi.org/10.1016/0304-3894(88)87014-6.
Bi, M., Ren, J., Zhao, B., Che, W., 2011. Effect of fire engulfment on thermal response of LPG tanks. J. Hazard. Mater. 192, 874–879. https://doi.org/10.1016/j.jhazmat.2011.05.107.
Birk, A.M., 1988. Modelling the response of tankers exposed to external fire impingement. J. Hazard. Mater. 20, 197–225. https://doi.org/10.1016/0304-3894(88)87013-4.
Birk, A.M., 1995. Scale effects with fire exposure of pressure-liquefied gas tanks. J. Loss Prev. Process Ind. 8, 275–290. https://doi.org/10.1016/0950-4230(95)00028-Y.
Birk, A.M., 2006. Fire Testing and Computer Modelling of Rail Tank-Cars Engulfed in Fires.
Birk, A.M., Cunningham, M.H., 1994. The boiling liquid expanding vapour explosion. J. Loss Prev. Process Ind. 7, 474–480. https://doi.org/10.1016/0950-4230(94)80005-7.
Birk, A.M., Poirier, D., Davison, C., 2006. On the response of 500gal propane tanks to a 25% engulfing fire. J. Loss Prev. Process Ind. 19, 527–541. https://doi.org/10.1016/j.jlp.2005.12.008.
Bradley, I., Scarponi, G.E., Otremba, F., Birk, A.M., 2021. An overview of test standards and regulations relevant to the fire testing of pressure vessels. Process Saf. Environ. Prot. 145, 150–156. https://doi.org/10.1016/J.PSEP.2020.07.047.
Bubbico, R., Mazzarotta, B., 2018. Dynamic response of a tank containing liquefied gas under pressure exposed to a fire: A simplified model. Process Saf. Environ. Prot. 113, 242–254. https://doi.org/10.1016/j.psep.2017.10.016.
Chi, Y., Liu, Z., Zhang, Y., 2015. UAV-based forest fire detection and tracking using digital processing techniques. Int. Conf. Unmanned Aircr. Syst. 639–643.
Clark, J.A., 1969. In: Irvine, T.F., Hartnett, J.P.B.T.-A. in H.T. (Eds.), Cryogenic Heat Transfer. Elsevier, pp. 325–517. https://doi.org/10.1016/S0065-2717(08)70132-1.
D'Aulisa, A., Tugnoli, A., Cozzani, V., Landucci, G., Birk, A.M., 2014. CFD modeling of LPG vessels under fire exposure conditions. AIChE J. 60, 4292–4305. https://doi.org/10.1002/aic.14599.
Dhanachandra, N., Manglem, K., Chanu, Y.J., 2015. Image Segmentation Using K-means Clustering Algorithm and Subtractive Clustering Algorithm. In: Procedia Computer Science. Elsevier, pp. 764–771. https://doi.org/10.1016/j.procs.2015.06.090.
Droste, B., Ulrich, A., Borch, J., 2011. Brand new fire test facilities at 'BAM test site technical safety. Packag. Transp. Storage Secur. Radioact. Mater. 22, 195–199.
Eskandari Torbaghan, M., Sasidharan, M., Reardon, L., Muchanga-Hvelplund, L.C.W., 2022. Understanding the potential of emerging digital technologies for improving road safety. Accid. Anal. Prev. 166. https://doi.org/10.1016/j.aap.2021.106543.
Graves, K.W., 1973. Development of a computer program for modeling the heat effects on a railroad tank car. No. FRA-OR&D 75-33 Final Rpt.
Hadjisophocleous, G.V., Sousa, A.C.M., Venart, J.E.S., 1990a. Mathematical modelling of LPG tanks subjected to full and partial fire engulfment. Int. J. Numer. Methods Eng. 30 (4), 629–646.
Hadjisophocleous, G.V., Sousa, A.C.M., Venart, J.E.S., 1990b. A study of the effect of the tank diameter on the thermal stratification in LPG tanks subjected to fire engulfment. J. Hazard. Mater. 25, 19–31. https://doi.org/10.1016/0304-3894(90)85067-D.
Huang, X., He, P., Rangarajan, A., Ranka, S., 2020. Intelligent intersection: two-stream convolutional networks for real-time near-accident detection in traffic video. ACM Trans. Spat. Algorithms Syst. 6. https://doi.org/10.1145/3373647.
Iannaccone, T., Scarponi, G.E., Landucci, G., Cozzani, V., 2021. Numerical simulation of LNG tanks exposed to fire. Process Saf. Environ. Prot. 149, 735–749. https://doi.org/10.1016/j.psep.2021.03.027.
Jie, A.C.H., Zamli, A.F.A., Zulkifli, A.Z.S., Yee, J.L.M., Lim, M., 2018. Flame analysis using image processing techniques. In: IOP Conference Series: Materials Science and Engineering. Institute of Physics Publishing. https://doi.org/10.1088/1757-899X/342/1/012060.
Jyoti Bora, D., Kumar Gupta, A., 2014. Effect of different distance measures on the performance of K-means algorithm: an experimental study in matlab. Int. J. Comput. Sci. Inf. Technol. 5 (2), 2501–2506.
Kansal, I., Popli, R., Verma, J., Bhardwaj, V., Bhardwaj, R., 2022. Digital Image Processing and IoT in Smart Health Care -A review. ESCI 2022 w, in: 2022 International Conference on Emerging Smart Computing and Informatics. Institute of Electrical and Electronics Engineers Inc. https://doi.org/10.1109/ESCI53509.2022.9758227.
Kim, J., Jo, D., 2023. Optimal camera placement to generate 3D reconstruction of a mixed-reality human in real environments. Electronics 12. https://doi.org/10.3390/electronics12204244.
Landucci, G., Molag, M., Reinders, J., Cozzani, V., 2009. Experimental and analytical investigation of thermal coating effectiveness for 3m3 LPG tanks engulfed by fire. J. Hazard. Mater. 161, 1182–1192. https://doi.org/10.1016/j.jhazmat.2008.04.097.
Lautkaski, R., 2009. Evaluation of BLEVE risks of tank wagons carrying flammable liquids. J. Loss Prev. Process Ind. 22, 117–123.
Leetaru, K., 2019. Using AI To Analyze Video As Imagery: The Impact Of Sampling Rate [WWW Document]. URL ⟨https://www.forbes.com/sites/kalevleetaru/2019/06/23/using-ai-to-analyze-video-as-imagery-the-impact-of-sampling-rate/⟩.
Leslie, I.R.M., Birk, A.M., 1991. State of the art review of pressure liquefied gas container failure modes and associated projectile hazards. J. Hazard. Mater. 28, 329–365. https://doi.org/10.1016/0304-3894(91)87083-E.
Li, Y., Huang, H., Shuai, J., Zhao, J., Su, B., 2018. Experimental study of continuously released liquid fuel spill fires on land and water in a channel. J. Loss Prev. Process Ind. 52, 21–28. https://doi.org/10.1016/j.jlp.2018.01.008.
Mahmoud, M.A.I., Ren, H., 2018. Forest fire detection using a rule-based image processing algorithm and temporal variation. Math. Probl. Eng. 2018. https://doi.org/10.1155/2018/7612487.
Makarov, D., Shentsov, V., Kuznetsov, M., Molkov, V., 2021. Hydrogen tank rupture in fire in the open atmosphere: hazard distance defined by fireball. Hydrogen 2, 134–146. https://doi.org/10.3390/hydrogen2010008.
Manjunatha, K.C., Mohana, H., Vijaya, P., 2015. Implementation of computer vision based industrial fire safety automation by using neuro-fuzzy algorithms. Int. J. Inf. Technol. Comput. Sci. 7, 14–27. https://doi.org/10.5815/ijitcs.2015.04.02.
Mata, C., Pastor, E., Rengel, B., Valero, M., Planas, E., Palacios, A., Casal, J., 2018. Infrared imaging software for jet fire analysis. Chem. Eng. Trans.
Mata, C., Walker, P.M., Oliver, A., Brunotte, F., Martí, J., Lalande, A., 2016. ProstateAnalyzer: web-based medical application for the management of prostate cancer using multiparametric MR imaging. Inform. Heal. Soc. Care 41, 286–306. https://doi.org/10.3109/17538157.2015.1008488.

Moodie, K., 1988. Experiments and modelling:- an overview with particular reference to fire engulfment. J. Hazard. Mater. 20, 149–175. https://doi.org/10.1016/0304-3894(88)87011-0.
Moodie, K., Billinge, K., Cutler, D.P., 1985. Fire engulfment of LPG storage tanks. Inst. Chem. Eng. Symp Ser. 87–106.
Moodie, K., Cowley, L.T., Denny, R.B., Small, L.M., Williams, I., 1988. Fire engulfment tests on a 5 tonne LPG tank. J. Hazard. Mater. 20, 55–71. https://doi.org/10.1016/0304-3894(88)87006-7.
Mu, Z., Jin, L., Yin, J., Wang, Q., 2022. Research on a driver fatigue detection model based on image processing. Hum. Centr Comput. Inf. Sci. 12. https://doi.org/10.22967/HCIS.2022.12.017.
Mutual, F., 1981. Approval Standard for Fire Protective Coatings for LP Gas Steel Storage Vessels and Process Structures.
National Fire and Protection Association, 2011. NFPA 58:Liquefied Petroleum Gas Code.
Ødegård, A., Sommerseth, C., Odsæter, L.H., Skarsvåg, H.L., Nekså, P., Meraner, C., Stølen, R., Li, T., Muthusamy Deiveegan, Van Wingerden, K., Siccama, D., Gawas, Y., Ustolin, F., George, C., 2022. D5.4: SH2IFT final project report.
Olague, G., Mohr, R., 2002. Optimal camera placement for accurate reconstruction. Pattern Recognit. 35, 927–944. https://doi.org/10.1016/S0031-3203(01)00076-0.
Pehr, K., 1996. Experimental examinations on the worst case behaviour of LH2/LNG tanks for passenger cars.
Pitas, I., 2000. Digital Image Processing Algorithms and Applications. John Wiley & Sons.
Plataniotis, K.N., Venetsanopoulos, A.N., 2000. Color Image Processing and Applications. Digital Signal Processing. Springer Berlin Heidelberg, Berlin, Heidelberg. https://doi.org/10.1007/978-3-662-04186-4.
Prabhakaran, A., Birk, M., Booth, G., 2018. Rail Tank. Car Total Contain. Fire Test.
Rahimian, P., Kearney, J.K., 2017. Optimal camera placement for motion capture systems. IEEE Trans. Vis. Comput. Graph 23, 1209–1221. https://doi.org/10.1109/TVCG.2016.2637334.
Rashidi, A., Ahmad, A., Lou, C., Hassan, H., Hariffin, M., Tzeng, M., Akma, N., Der, S., 2015. Preliminary determination of flame speeds from infrared images using image processing techniques in a 150 kWth coal fired combustion test rig. Inst. Res. Eng. Dr. LLC 1–5. https://doi.org/10.15224/978-1-63248-072-9-50.
Russ, J.C., 2006. The Image Processing Handbook, Fifth Edition. ed. CRC Press.
Scarponi, G.E., Cozzani, V., Antonioni, G., Doghieri, F., 2024. Modeling the behavior of LPG tanks exposed to partially engulfing pool fires. Process Saf. Environ. Prot. 182, 1072–1085. https://doi.org/10.1016/j.psep.2023.12.048.
Scarponi, G.E., Landucci, G., Birk, A.M., Cozzani, V., 2018a. LPG vessels exposed to fire: scale effects on pressure build-up. J. Loss Prev. Process Ind. 56, 342–358. https://doi.org/10.1016/j.jlp.2018.09.015.
Scarponi, G.E., Landucci, G., Birk, A.M., Cozzani, V., 2021. Three dimensional CFD simulation of LPG tanks exposed to partially engulfing pool fires. Process Saf. Environ. Prot. 150, 385–399.
Scarponi, G.E., Landucci, G., Heymes, F., Cozzani, V., 2018b. Experimental and numerical study of the behaviour of LPG tanks exposed to wildland fires. Process Saf. Environ. Prot. 114, 251–270.
Seeram, E., 2019. Digital Image Processing Concepts. In: Digital Radiography. Springer, Singapore, pp. 21–39.
Sharma, A., Singh, P.K., Kumar, Y., 2020. An integrated fire detection system using IoT and image processing technique for smart cities. Sustain. Cities Soc. 61, 102332. https://doi.org/10.1016/j.scs.2020.102332.
Shebeko, Y.N., Shevchuck, A.P., Smolin, I.M., 1996. BLEVE prevention using vent devices. J. Hazard. Mater. 50, 227–238. https://doi.org/10.1016/0304-3894(96)01777-3.
Sinaga, K.P., Yang, M.S., 2020. Unsupervised K-means clustering algorithm. IEEE Access 8, 80716–80727. https://doi.org/10.1109/ACCESS.2020.2988796.
Singh, G., Mittal, A., 2014. Various image enhancement techniques-a critical review. Int. J. Innov. Sci. Res.
Sumathipala, U.K., Hadjisophocleous, G.V., Aydemir, N.U., Yu, C.-M., Sousa, A.C.M., Steward, F.R., Venart, J.E.S., 1992. Fire engulfment of pressure-liquefied gas tanks: experiments and modeling. Fire Hazard Fire Risk Assess. 1150, 100–111.
Townsend, W., Anderson, C., Zook, J., Cowgill, G., 1974. Comparison of Thermally Coated and Uninsulated Rail Tank Cars Filled With LPG Subjected to a Fire Environment.
Turan, G., Guota, S., 2013. Road accidents prevention system usingdriver's drowsiness detection. Int. J. Adv. Res. Comput. Eng. Technol. 2.
Ustolin, F., Scarponi, G.E., Iannaccone, T., Cozzani, V., Paltrinieri, N., 2022. Cryogenic hydrogen storage tanks exposed to fires: a CFD study. Chem. Eng. Trans. 90, 535–540. https://doi.org/10.3303/CET2290090.
Wang, M., Wang, J., Yu, X., Zong, R., 2023. Experimental and numerical study of the thermal response of a diesel fuel tank exposed to fire impingement. Appl. Therm. Eng. 227, 120334. https://doi.org/10.1016/j.applthermaleng.2023.120334.
Yoon, K.T., Birk, A.M., 2004. Computational fluid dynamics analysis of local heating of propane tanks.
Zhou, H., Tang, Q., Yang, L., Yan, Y., Lu, G., Cen, K., 2014. Support vector machine based online coal identification through advanced flame monitoring. Fuel 117, 944–951. https://doi.org/10.1016/j.fuel.2013.10.041.